Measuring Mobile Trajectory Geometric Similarity Based on Discrete Positioning Points

Zhixiu Liu, Ziyang Deng, and Zihao Guo

Abstract—The assessment of similarity among mobile trajectories plays an important role in trajectory data mining. Trajectory similarity is a vague concept, and there is no precise metric, where the geometric similarity of the trajectories has received more attention. Considering the commonly used Hausdorff and Fréchet distances as measures, there is a process of traversal calculation to match the corresponding points or parts of two trajectories, which is computationally expensive and cannot reflect the geometric similarity of the trajectory commendably. By using deep learning technology to approximate or extract the features of the trajectory, the measure of trajectory similarity depends on the quality and scale of the data. Meanwhile, it is difficult to explain the geometric significance of the abstract features of the trajectory extracted by deep learning technology. In view of this, this study proposes the concepts of local shape matrix and merged shape matrices for characterizing the local and overall shapes of moving trajectories. The symbol overlap method for the merged shape matrix is also proposed to match the corresponding points or parts of the two trajectories. Both theoretical analysis and experiments show that the proposed shape matrix and symbol overlap method can be effectively used to measure the geometric similarity of moving trajectories based on discrete positioning points.

Index Terms—Trajectory Similarity; Shape Matrix; Symbol Overlap Method; Hausdorff Distance; Fréchet Distance; Deep Representation Techniques

I. INTRODUCTION

ITH the widespread adoption of satellite positioning applications and services, the acquisition and utilization of positioning data have become increasingly convenient. As is well known, we commonly gather satellite-based location data for mobile objects (such as vehicles, ships, and mobile robots) at discrete time intervals. Consequently, the positioning data employed are typically characterized by their discrete nature. The investigation of similarity among mobile trajectories based on such discrete positioning data has emerged as a critical focal point in the realm of trajectory information mining [1-2]. This research holds significant practical implications, as it

Manuscript received May 25, 2025; revised September 10, 2025.

This work was supported by the Jiangxi Province University Humanities and Social Sciences Research Project (JY22202).

Zhixiu Liu is a lecturer at the School of Science, Jiangxi University of Water Resources and Electric Power, Nanchang 330099, China (E-mail: zhixiuliu82@qq.com).

Ziyang Deng is a postgraduate student of the School of Mathematics and Computer Science, Nanchang University, Nanchang 330099, China (E-mail: zia399@email.ncu.edu.cn).

Zihao Guo is a postgraduate student at the School of Science, Jiangxi University of Water Resources and Electric Power, Nanchang 330099, China (E-mail: 3218392366@qq.com).

provides essential underpinning for various applications, including trajectory search, anomaly detection, target tracking, path planning, and navigation [3-6]. In fact, the study of trajectory similarity proves to be an exceedingly open-ended inquiry, seemingly devoid of singular evaluative criteria. Numerous distinct research methodologies and perspectives exist, often contingent on their ability to address practical challenges. In terms of primary research methodologies of the geometric similarity of the trajectories, they can broadly be categorized into two classes [7-11]: those centered on "computing distances between curves" and those involving "fitting or approximating curves and their features."

Evidently, the movement trajectories can be regarded as spatial curves (point sets). The similarity of two curves generally refers to geometric similarity. The notion of two curves, C and \tilde{C} , being similar implies the existence of a certain one-to-one correspondence between the points of curve C and those of curve C. In other words, the ratio between the line segments connecting any two points on curve C and the corresponding line segments connecting two points on curve is constant, as illustrated in Fig. 1.

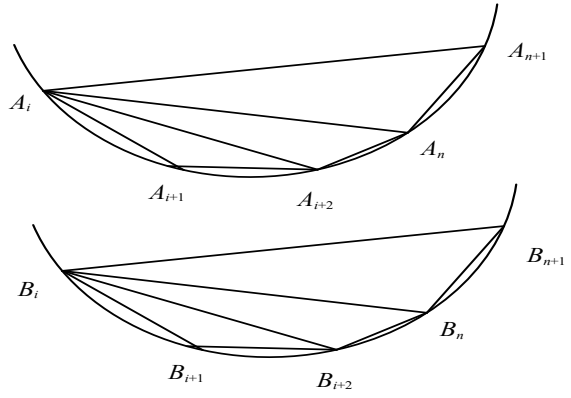


Fig. 1. Illustration of the curve similarity.

For smooth curves, we have some criteria for determining curve similarity [12-13]. However, in practice, it is often challenging to find two curves, especially those derived from real-world scenarios, that are entirely similar. Instead, our primary focus is on quantifying the differences or degree of similarity between two given curves. This is a complex and open-ended problem that lacks a widely accepted similarity metric. Currently, it is addressed to a certain extent and within specific contexts. Even continuous plane curves can exhibit highly intricate forms that are challenging to measure in terms of their similarities. For example, consider the Weierstrass function, which is nowhere differentiable and has a dimension exceeding 1, or the Peano curve, which fills the entire square region [14-15]. The problem becomes even more intricate when dealing with similarity measurements for curves in general three-dimensional spaces. Currently, the most commonly used distance-based methods for measuring curve or mobile trajectory similarity include L^p distance, Hausdorff distance, Fréchet distance, and their various derivatives [16-20]. Considering their original definitions (which have corresponding discrete forms for practical computation and various variations that remain rooted in their essence), it is evident that these methods involve traversing computations to establish correspondence between points or parts on two trajectories. This results in high computational complexity, with relatively less emphasis on capturing the "shape" similarity of trajectories.

Definition A (L^p distance) [16] Given two trajectories, denoted as $C_A(t)$ and $C_B(t)$, $t \in [0,1]$, their L^p distance is defined as

$$d_{L^{p}}(C_{A}, C_{B}) = \left(\int_{0}^{1} |C_{A}(t) - C_{B}(t)|^{p} dt\right)^{\frac{1}{p}}.$$
 (1)

Given a threshold $\varepsilon > 0$, when $d_{L^p}(C_A, C_B) \le \varepsilon$, we consider trajectories $C_A(t)$ and $C_B(t)$ to be similar. Conversely, we regard them as being dissimilar.

Upon close examination, a natural question arises: are points $C_A(t)$ and $C_B(t)$ on the aforementioned trajectories correctly matched as corresponding points? If the matching of the corresponding points is misaligned, it will result in different L^p distances. As illustrated in Fig. 2, consider trajectories C_A and C_B , both consisting of straight-line segments but with different point correspondences. It is evident that the calculated L^p distances would differ.

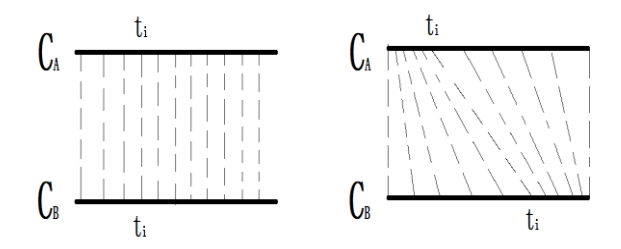


Fig. 2. Different correspondences of matching points in two trajectories

The optimal point correspondence between the two trajectories can be determined through an exhaustive search, allowing for the correction of the distance between the two trajectories to be expressed as

$$d_{L^p}(C_A, C_B) = \inf_{\alpha, \beta} \left(\int_0^1 |C_A(\alpha(s)) - C_B(\beta(s))|^p ds \right)^{\frac{1}{p}} \tag{2}$$

where $\alpha(s)$ and $\beta(s)$ encompass all continuous non-decreasing real functions, satisfying $\alpha(0) = \beta(0) = 0$ and $\alpha(1) = \beta(1) = 1$. It is evident that such exhaustive traversal computations would be prohibitively expensive and may even be infeasible to implement. Furthermore, as illustrated in Fig. 3, it is apparent that two curves with significantly different shapes can still have equal L^p distances from the same reference curve. This underscores the limitation of distance in adequately capturing the shapes of the curves. Now, let us examine the commonly used Hausdorff and Fréchet distances.

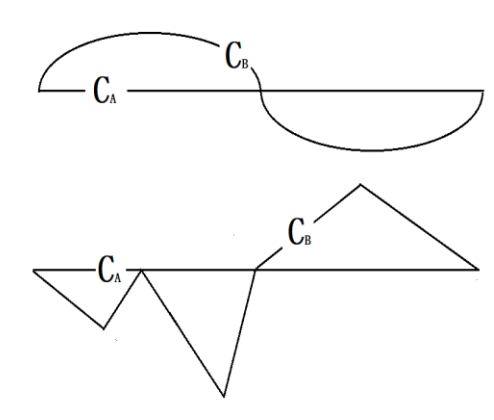


Fig. 3. Two sets of curves with equal distances but significant shape differences

Definition B (Hausdorff distance) [10] Given two trajectories, denoted as $C_A(t)$ and $C_B(t)$, $t \in [0,1]$, their Hausdorff distance is defined as follows:

$$d_H(C_A, C_B) = \max \left\{ \max_{a \in C_A(t)} \min_{b \in C_B(t)} ||a - b||, \max_{b \in C_B(t)} \min_{a \in C_A(t)} ||a - b|| \right\}.$$
 (3) **Definition C** (Fréchet distance) [11] Given two trajectories,

Definition C (Fréchet distance) [11] Given two trajectories denoted as $C_A(t)$ and $C_B(t)$, $t \in [0,1]$, their Fréchet distance is defined as follows:

$$d_F(C_A, C_B) = \inf_{\alpha, \beta} \max_{s \in [0,1]} \left\| C_A(\alpha(s)) - C_B(\beta(s)) \right\| \tag{4}$$

where $\alpha(s)$ and $\beta(s)$ encompass all continuous non-decreasing real functions, satisfying $\alpha(0) = \beta(0) = 0$ and $\alpha(1) = \beta(1) = 1$.

The aforementioned Hausdorff and Fréchet distances both entail exhaustive computations involving the selection of maximum or minimum values. One of the critical rationales behind this approach is to ensure proper pairing of corresponding points or parts between two trajectories. For instance, in the case of the Hausdorff distance, the $\min_{b \in C_B(t)} \|a - b\|$

operation aims to locate the most suitable corresponding

point in trajectory $C_B(t)$ for a given point a. Similarly, in the context of the Fréchet distance, the use of $\inf_{\alpha,\beta}$, as previously discussed in the context of the corrected L^p distance, serves the purpose of appropriately matching the corresponding points between the two curves. Consequently, these computations incur substantial computational overheads. Furthermore, both distance metrics are based on point-to-point distances and do not provide a comprehensive reflection of the geometric shapes and characteristics of the trajectories. As illustrated in Fig. 4, consider the curves C_{A_n} constructed from the two oblique sides of a regular triangle and C_B , which is a straight line segment. Notably, the Hausdorff and Fréchet distances between curve C_{A_n} and line C_{B} both steadily decrease towards zero($n \rightarrow \infty$). However, it is crucial to recognize that curve C_{A_n} is consistently twice as long as C_B . Their geometric shapes inherently differ significantly, since C_A is a zigzag shape but C_B is a straight line shape [21].

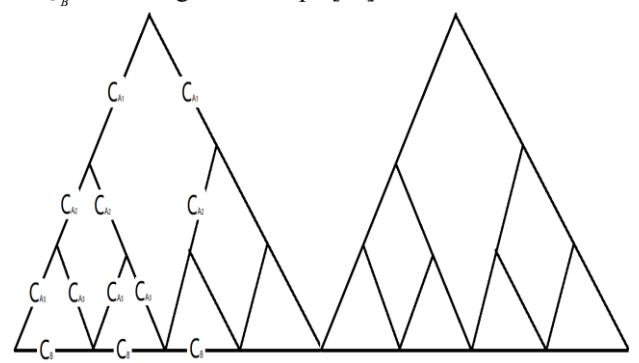


Fig. 4. Two sets of curves with distances tending to infinitesimally, differing in length by a factor of two.

In addition to the distance-based methods discussed earlier for measuring trajectory similarity by calculating the distances between two curves, there are approaches that involve curve and their characteristics fitting and approximation, notably the well-known deep learning methods [22-23]. These techniques typically involve approximating curves or abstracting their features using deep learning methodologies and subsequently employing these representations to measure curve similarity. For example, applications such as deep learning-based handwritten digit recognition [24-25] and deep learning-based mobile trajectory similarity analysis [7-8,26] are fundamentally aimed at measuring curve similarity. However, the use of deep learning methods to measure trajectory similarity is heavily dependent on the quality and scale of the trajectory data. Furthermore, these methods often lack interpretability, making it challenging to easily attribute geometric significance to the abstract features extracted from the trajectories using deep learning techniques.

Considering the limitations of using distance-based methods, which involve computationally expensive point matching through traversal, and the challenges associated with deep learning techniques for trajectory similarity measurement, where data quality and quantity requirements are high and interpretability is limited, this study introduces the concept of "local shape matrices" to describe the local shapes of mobile trajectories. Additionally, it presents the concept of "merged shape matrices" for characterizing the overall shape of curves. The proposed methodology utilizes the "merged shape matrix," "negative merged shape matrix," "inverse merged shape matrix," and "negative inverse merged shape matrix" from one trajectory, overlapped with the "merged shape matrix" of another trajectory, employing a "symbol overlap method" to match the corresponding points or parts on the two trajectories (i.e., the maximum number of matching points where the signs of the values at overlapping positions in the two matrices are the same). This approach circumvents complex traversal computations, effectively aligns the corresponding points or parts on the trajectories, and does not require an abundance of trajectory data to train deep representation models. The subsequent sections (Sections Two and Three) delineate the mobile trajectory similarity measurement methodology proposed in this paper, while Section Four computes and visually validates the similarity levels of various mobile trajectories based on discrete positioning data[27-29].

II. SHAPE MATRICES FOR MOBILE TRAJECTORIES

A. Local Bending Direction of Mobile Trajectories -Characterized by the Sign of Triangle Algebraic Area

Given a set of points on a planar trajectory, assuming that the trajectory runs from A to F , as depicted in Fig. 5, we examined the bending direction of contiguous sets of three points, such as ABC and DEF, within this trajectory segment. Let the coordinates of points A, B, C, D, E, and F be denoted as $(x_A, y_A), (x_B, y_B), (x_C, y_C), (x_D, y_D), (x_E, y_E)$ and (x_F, y_F) , respectively. The algebraic area of triangle ABC is calculated as follows:

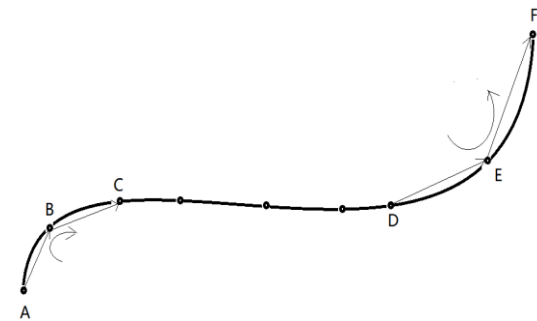


Fig. 5. Illustration of local bending directions in the trajectories.

$$\begin{vmatrix} x_A & y_A \\ x_B & y_B \end{vmatrix} + \begin{vmatrix} x_B & y_B \\ x_C & y_C \end{vmatrix} + \begin{vmatrix} x_C & y_C \\ x_A & y_A \end{vmatrix}$$

The algebraic area of triangle DEF can be computed as

$$\begin{vmatrix} x_{\mathrm{D}} & y_{\mathrm{D}} \\ x_{E} & y_{E} \end{vmatrix} + \begin{vmatrix} x_{E} & y_{E} \\ x_{F} & y_{F} \end{vmatrix} + \begin{vmatrix} x_{F} & y_{F} \\ x_{D} & y_{D} \end{vmatrix}$$

Here, we are primarily concerned with the sign of the algebraic area, as it signifies the relative positions of the three vertices of the triangle. As shown in Fig. 5,

$$\operatorname{sgn}\begin{bmatrix} \begin{vmatrix} x_A & y_A \\ x_B & y_B \end{vmatrix} + \begin{vmatrix} x_B & y_B \\ x_C & y_C \end{vmatrix} + \begin{vmatrix} x_C & y_C \\ x_A & y_A \end{bmatrix} < 0$$

signifying that points A, B, and C form a clockwise orientation.

$$\operatorname{sgn}\begin{bmatrix} \left| x_{\mathrm{D}} & y_{D} \right| + \left| x_{E} & y_{E} \right| + \left| x_{F} & y_{F} \right| \\ x_{E} & y_{E} & y_{F} & y_{F} \end{bmatrix} > 0$$

indicating that points D, E, and F form a counterclockwise orientation. Consequently, the sign of the algebraic area of the triangle formed by three adjacent points on the mobile trajectory represents the local bending direction of the trajectory segment. In the mathematical expression above,

$$\operatorname{sgn}[z] = \begin{cases} +1 & z > 0 \\ 0 & z = 0 \\ -1 & z < 0 \end{cases}$$

denotes the sign function, where the | | within the brackets represents the determinant. It is important to note that in other parts of this paper, | | may denote the absolute value.

Remark 1 In practical applications, due to inherent data errors, the true value of the algebraic area of the triangle formed by adjacent three points on a trajectory is unlikely to

be precisely zero, even if the triangle degraded into a straight line segment. Therefore, it is customary to establish a very small positive value, denoted \mathcal{E} as a threshold instead of zero to adjust sgn[z]. Thus, sgn[z] is replaced with

$$\operatorname{sgn}[z] = \begin{cases} +1 & z > \varepsilon \\ 0 & -\varepsilon < z < \varepsilon, \\ -1 & z < -\varepsilon \end{cases}$$
 (5)

it is employed to determine the sign of the algebraic area of the triangle formed by the adjacent three points, effectively indicating the local bending direction of the trajectory.

Remark 2 For trajectories in three-dimensional space, it is agreed that the positive z direction is upward vertical to ground, and the x and y directions are determined according to the right-hand rule. The trajectories can be projected onto an x-y coordinate plane, and their local bending direction can be determined based on the plane coordinates of the projected trajectory. As illustrated in Fig. 6, the z-coordinates of points A and C are greater than that of point B, projecting points A, B, and C onto A', B', and C' allows us to ascertain the local bending direction of the original trajectory based on the observation direction of points A', B', and C'.

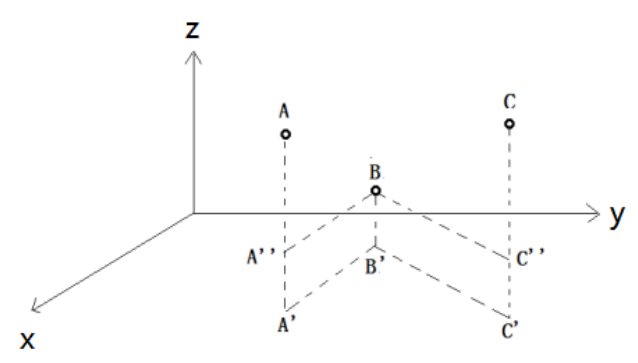


Fig. 6. Projection of points from spatial trajectories onto the plane.

B. Local Horizontal Bending Degree of Mobile Trajectories - Characterized by the Ratio of Triangle Side Lengths

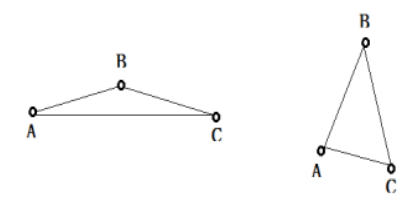


Fig. 7. Bending Degree of points along the trajectory.

As shown in Fig. 7, with three points $A(x_4, y_4)$, B (x_B, y_B) , and $C(x_C, y_C)$ on a mobile trajectory, it is evident that angle B on the left is greater than angle B on the right. By utilizing the Law of Cosines for triangles, we can represent the cosine value of angle B as follows:

$$\cos \angle B = \frac{|AB|^2 + |BC|^2 - |AC|^2}{2|AB||BC|}$$
 (6)

The larger the value in the equation, the smaller the angle B, indicating a more pronounced bending at point B on the

trajectory. Conversely, a smaller value in the equation corresponds to a larger angle B, indicating a lesser degree of bending at point B. Therefore, we can use the following expression to represent the bending degree at point B on the trajectory:

$$\frac{|AB|^{2} + |BC|^{2} - |AC|^{2}}{2|AB||BC|}$$
 (7)

If the sampling points on the trajectory are uniformly spaced, meaning that they are sampled based on equal arc lengths (which is approximately the case for constant velocity moving object trajectories based on satellite positioning at equal interval times), for the sake of computational convenience, it is also possible to directly use

$$\frac{\left|AB\right| + \left|BC\right|}{\left|AC\right|} \tag{8}$$

to characterize the bending degree at point B of the trajectory. Clearly, the larger the value in the expression, the smaller the angle B, indicating more pronounced bending at point B on the trajectory. Conversely, a smaller value in the expression results in a larger angle B, signifying a lesser degree of bending at point B.

Due to

$$\frac{|AB|^{2} + |BC|^{2} - |AC|^{2}}{2|AB|BC|} = \frac{\left[(x_{B} - x_{A})^{2} + (y_{B} - y_{A})^{2} \right] + \left[(x_{C} - x_{B})^{2} + (y_{C} - y_{B})^{2} \right] - \left[(x_{C} - x_{A})^{2} + (y_{C} - y_{A})^{2} \right]^{2}}{2\left[(x_{B} - x_{A})^{2} + (y_{B} - y_{A})^{2} \right]^{\frac{1}{2}} \left[(x_{C} - x_{B})^{2} + (y_{C} - y_{B})^{2} \right]^{\frac{1}{2}}}
\frac{|AB| + |BC|}{|AC|} = \frac{\left[(x_{B} - x_{A})^{2} + (y_{B} - y_{A})^{2} \right]^{\frac{1}{2}} + \left[(x_{C} - x_{B})^{2} + (y_{C} - y_{B})^{2} \right]^{\frac{1}{2}}}{\left[(x_{C} - x_{A})^{2} + (y_{C} - y_{A})^{2} \right]^{\frac{1}{2}}}$$
(9)
In summary, it is possible to utilize

$$sgn\left[\begin{vmatrix} x_{A} & y_{A} \\ x_{B} & y_{B} \end{vmatrix} + \begin{vmatrix} x_{B} & y_{B} \\ x_{C} & y_{C} \end{vmatrix} + \begin{vmatrix} x_{C} & y_{C} \\ x_{A} & y_{A} \end{vmatrix}\right]$$

$$\frac{\left[(x_{B} - x_{A})^{2} + (y_{B} - y_{A})^{2}\right] + \left[(x_{C} - x_{B})^{2} + (y_{C} - y_{B})^{2}\right] - \left[(x_{C} - x_{A})^{2} + (y_{C} - y_{A})^{2}\right]}{2\left[(x_{C} - x_{A})^{2} + (y_{C} - y_{B})^{2}\right]^{\frac{1}{2}}}$$

or

$$\operatorname{sgn}\left[\begin{vmatrix} x_{A} & y_{A} \\ x_{B} & y_{B} \end{vmatrix} + \begin{vmatrix} x_{B} & y_{B} \\ x_{C} & y_{C} \end{vmatrix} + \begin{vmatrix} x_{C} & y_{C} \\ x_{A} & y_{A} \end{vmatrix}\right]$$

$$\frac{\left[(x_{B} - x_{A})^{2} + (y_{B} - y_{A})^{2}\right]^{\frac{1}{2}} + \left[(x_{C} - x_{B})^{2} + (y_{C} - y_{B})^{2}\right]^{\frac{1}{2}}}{\left[(x_{C} - x_{A})^{2} + (y_{C} - y_{A})^{2}\right]^{\frac{1}{2}}}$$
(10)

denotes the direction and degree of bending at point B on the trajectory.

Remark 3 Similar to Remark 2, if the mobile trajectory is in three-dimensional space, it can be projected onto the x-y coordinate plane, as shown in Fig. 6. Subsequently, the local bending degree of the trajectory can be determined based on the plane coordinates of the points on the projected trajectory.

C. Local Vertical Steepness Direction and Degree of Mobile Trajectories - Characterized by the Ratio of Triangle Side Lengths

Building on Remarks 2 and 3, we previously discussed the characterization of the local bending direction and degree of spatial trajectories in the horizontal direction. Now, let us address the characterization of the local vertical steepness direction and degree of the trajectories. For local spatial trajectories, such as points A, B, and C in Fig.6, let's denote the coordinates of points A, B, and C as (x_4, y_4, z_4) , (x_B, y_B, z_B) , and (x_C, y_C, z_C) , respectively. Since the tangent value of angle B in right triangle $\Delta AA''B$ characterizes the slope direction and degree of side AB, we can use

$$\frac{AA''}{|A''B|} = \frac{AA''}{|A'B'|} = \frac{z_B - z_A}{\left[(x_B - x_A)^2 + (y_B - y_A)^2 \right]^{\frac{1}{2}}}$$
(11)

to represent the vertical steepness variation from point A to point B along the trajectory. Similarly, we can use

$$\frac{C''C}{|BC''|} = \frac{C''C}{|B'C'|} = \frac{z_C - z_B}{\left[(x_C - x_B)^2 + (y_C - y_B)^2 \right]^{\frac{1}{2}}}$$
(12) to represent the vertical steepness variation from point B to

point C along the trajectory.

As shown in Fig. 6, when

$$\frac{AA''}{|A''B|} = \frac{AA''}{|A'B|} = \frac{z_B - z_A}{\left[(x_A - x_B)^2 + (y_A - y_B)^2 \right]^{\frac{1}{2}}}$$
(13)

direction from point A to point B. Conversely, when

$$\frac{C''C}{|BC''|} = \frac{C''C}{|B'C'|} = \frac{z_C - z_B}{\left[(x_C - x_B)^2 + (y_C - y_B)^2 \right]^{\frac{1}{2}}}$$
is greater than 0, it indicates an increase in vertical direction

from point B to point C. The absolute values of these tangent values correspond to the steepness of the local trajectory, with larger absolute values denoting steeper segments.

Remark 4 Similar to Remark 1, the threshold for determining whether the local trajectory is ascending or descending vertically, denoted as 0, should typically be replaced with a positive value \mathcal{E} in practice. This adjustment accounts for the presence of errors in the real data. Even if points A, B, and C lie in the same plane, their differences in the z-coordinates are usually not exactly 0, but rather a relatively small value.

D. Local Shape of Mobile Trajectories - Characterized by Local Shape Matrices

Previously, we described the horizontal bending direction and degree, as well as the vertical steepness direction and degree of the local trajectory around points A, B, and C. Combining these aspects, we can use a three-dimensional vector, denoted as

$$\operatorname{sgn} \begin{bmatrix} x_{A} & y_{A} \\ x_{B} & y_{B} \end{bmatrix} + \begin{vmatrix} x_{B} & y_{B} \\ x_{C} & y_{C} \end{vmatrix} + \begin{vmatrix} x_{C} & y_{C} \\ x_{A} & y_{A} \end{bmatrix} \underbrace{ \begin{vmatrix} (x_{B} - x_{A})^{2} + (y_{B} - y_{A})^{2} \\ 2((x_{B} - x_{A})^{2} + (y_{C} - y_{B})^{2})^{2} \underbrace{ \begin{vmatrix} (x_{C} - x_{B})^{2} + (y_{C} - y_{B})^{2} \\ 2((x_{B} - x_{A})^{2} + (y_{B} - y_{A})^{2})^{2} \underbrace{ \begin{vmatrix} (x_{C} - x_{B})^{2} + (y_{C} - y_{B})^{2} \\ (x_{C} - x_{B})^{2} + (y_{C} - y_{B})^{2} \underbrace{ \begin{vmatrix} (x_{C} - x_{B})^{2} + (y_{C} - y_{B})^{2} \\ (x_{C} - x_{B})^{2} + (y_{C} - y_{B})^{2} \underbrace{ \begin{vmatrix} (x_{C} - x_{B})^{2} + (y_{C} - y_{B})^{2} \\ (x_{C} - x_{B})^{2} + (y_{C} - y_{B})^{2} \underbrace{ \begin{vmatrix} (x_{C} - x_{B})^{2} + (y_{C} - y_{B})^{2} \\ (x_{C} - x_{B})^{2} + (y_{C} - y_{B})^{2} \underbrace{ \begin{vmatrix} (x_{C} - x_{B})^{2} + (y_{C} - y_{B})^{2} \\ (x_{C} - x_{B})^{2} + (y_{C} - y_{B})^{2} \underbrace{ \begin{vmatrix} (x_{C} - x_{B})^{2} + (y_{C} - y_{B})^{2} \\ (x_{C} - x_{B})^{2} + (y_{C} - y_{B})^{2} \underbrace{ \begin{vmatrix} (x_{C} - x_{B})^{2} + (y_{C} - y_{B})^{2} \\ (x_{C} - x_{B})^{2} + (y_{C} - y_{B})^{2} \underbrace{ \begin{vmatrix} (x_{C} - x_{B})^{2} + (y_{C} - y_{B})^{2} \\ (x_{C} - x_{B})^{2} + (y_{C} - y_{B})^{2} \underbrace{ \begin{vmatrix} (x_{C} - x_{B})^{2} + (y_{C} - y_{B})^{2} \\ (x_{C} - x_{B})^{2} + (y_{C} - y_{B})^{2} \underbrace{ \begin{vmatrix} (x_{C} - x_{B})^{2} + (y_{C} - y_{B})^{2} \\ (x_{C} - x_{B})^{2} + (y_{C} - y_{B})^{2} \underbrace{ \begin{vmatrix} (x_{C} - x_{B})^{2} + (y_{C} - y_{B})^{2} \\ (x_{C} - x_{B})^{2} + (y_{C} - y_{B})^{2} \underbrace{ \begin{vmatrix} (x_{C} - x_{B})^{2} + (y_{C} - y_{B})^{2} \\ (x_{C} - x_{B})^{2} + (y_{C} - y_{B})^{2} \underbrace{ \begin{vmatrix} (x_{C} - x_{B})^{2} + (y_{C} - y_{B})^{2} \\ (x_{C} - x_{B})^{2} + (y_{C} - y_{B})^{2} \underbrace{ \begin{vmatrix} (x_{C} - x_{B})^{2} + (y_{C} - y_{B})^{2} \\ (x_{C} - x_{B})^{2} + (y_{C} - y_{B})^{2} + (y_{C} - y_{B})^{2} \underbrace{ \begin{vmatrix} (x_{C} - x_{B})^{2} + (y_{C} - y_{B})^{2} \\ (x_{C} - x_{B})^{2} + (y_{C} - y_{B})^{2} + (y_{C} - y_{C})^{2} + (y_{C} - y_{C})^{2} + (y_{C} - y_{C})$$

$$\left(\operatorname{sgn}\begin{bmatrix} x_{A} & y_{A} \\ x_{B} & y_{B} \end{bmatrix} + \begin{vmatrix} x_{B} & y_{B} \\ x_{C} & y_{C} \end{bmatrix} + \begin{vmatrix} x_{C} & y_{C} \\ x_{A} & y_{A} \end{bmatrix} \frac{\left[(x_{B} - x_{A})^{2} + (y_{B} - y_{A})^{2}\right]^{\frac{1}{2}} + \left[(x_{C} - x_{B})^{2} + (y_{C} - y_{B})^{2}\right]^{\frac{1}{2}}}{\left[(x_{C} - x_{A})^{2} + (y_{C} - y_{A})^{2}\right]^{\frac{1}{2}}} \frac{z_{B} - z_{A}}{\left[(x_{A} - x_{B})^{2} + (y_{A} - y_{B})^{2}\right]^{\frac{1}{2}}}}{\left[(x_{C} - x_{B})^{2} + (y_{C} - y_{B})^{2}\right]^{\frac{1}{2}}} \right) \tag{15}$$

to characterize the local shape of the trajectory near point B. This vector is referred to as the "local shape vector" and is denoted as $(S_1 \ S_2 \ S_3)^T$, where S_1 , S_2 , and S_3 represent the first, second, and third components of the vector in expression (15).

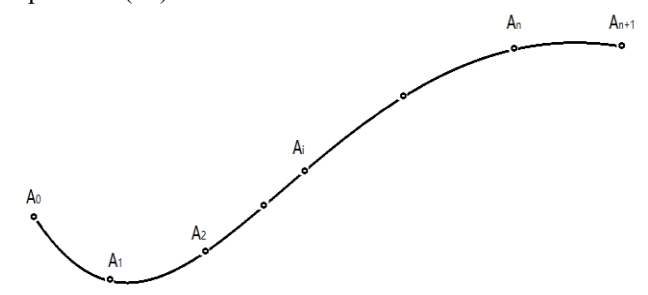


Fig. 8. Multiple sampling points on mobile trajectory.

For any three adjacent sampling points on the mobile trajectory, a corresponding local shape vector can be computed based on expression (15). These local shape vectors, determined by all sets of adjacent three sampling points except for the initial and final points, are arranged sequentially into a matrix denoted as

$$\begin{pmatrix}
S_1^1 & S_1^2 & \cdots & S_1^{n-1} & S_1^n \\
S_2^1 & S_2^2 & \cdots & S_2^{n-1} & S_2^n \\
S_3^1 & S_3^2 & \cdots & S_3^{n-1} & S_3^n
\end{pmatrix}_{3\times n}$$
(16)

We refer to this matrix as the "local shape matrix" of the mobile trajectory. As illustrated in the diagram in Fig. 8, the first column represents the local shape vectors calculated from A_0, A_1, A_2 , the second column from A_0, A_1, A_2 , and so forth, with the last column showing the local shape vectors calculated from A_{n-1}, A_n, A_{n+1} .

E. Global Shape of Mobile Trajectories - Characterized by Merged Shape Matrices

It is discernible that the vector formed by the signs of the components in the local shape vector, which we refer to as the "symbol vector", encapsulates the approximate local shape of the trajectory. This pertains to both the horizontal bending direction and the vertical ascent or descent orientation. The magnitude of the numerical values following the symbols (omitted here for brevity) denotes the degree of horizontal bending and the steepness of the vertical direction, as illustrated in Fig. 9.

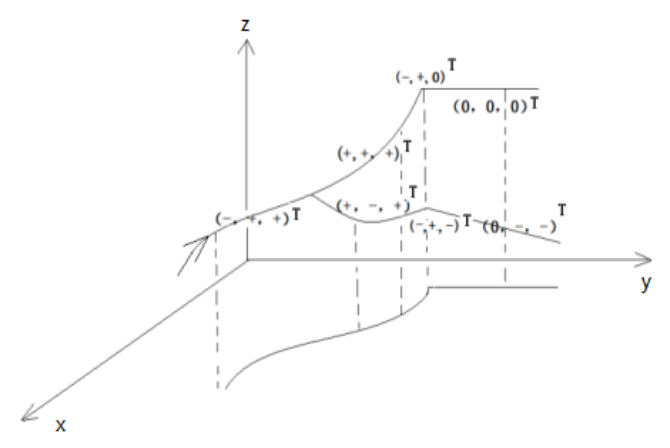


Fig. 9. The corresponding symbol vectors for local shape vectors and their significance

Consequently, when the symbol vectors of adjacent local shape vectors within the local shape matrix are identical, it signifies that they share a common horizontal bending and vertical ascent/descent direction. This indicates the continuation of the same shape pattern, which can be aggregated and accumulated to represent broader shape characteristics of the particles. In other words, if every component of both $S_1^i S_2^i S_3^i$ and $S_3^{i+1} S_2^{i+1} S_3^{i+1}$ shares the same sign, they are merged into a new vector $S_1^i + S_1^{i+1} S_2^i + S_2^{i+1} S_3^i + S_3^{i+1}$, and the merging process continues until no further merging is possible between adjacent columns. The resulting matrix, denoted as

$$\begin{pmatrix}
S_{1}^{\tilde{1}} & S_{1}^{\tilde{2}} & \cdots & S_{1}^{\tilde{n}} \\
S_{2}^{\tilde{1}} & S_{2}^{\tilde{2}} & \cdots & S_{2}^{\tilde{n}} \\
S_{3}^{\tilde{1}} & S_{3}^{\tilde{2}} & \cdots & S_{3}^{\tilde{n}}
\end{pmatrix}_{3\times\tilde{n}}$$
(17)

is referred to as the "merged shape matrix." It offers a deeper insight into the overall shape of the mobile trajectory, often with $\widetilde{n} \leq n$.

III. SYMBOL OVERLAP APPROACH FOR CORRESPONDENCE MATCHING AND TRAJECTORY SIMILARITY

A. Different Perspectives on Mobile Trajectories -Represented with Negative, Inverse, and Negative-Inverse Merged Shape Matrices

When examining mobile trajectories from alternative vantage points, we may encounter scenarios where the signs and order of the local shape vector components are reversed. Consequently, we designate the matrices

$$\begin{pmatrix}
-S_{1}^{\tilde{1}} & -S_{1}^{\tilde{2}} & \cdots & -S_{1}^{\tilde{n}} \\
-S_{2}^{\tilde{1}} & -S_{2}^{\tilde{2}} & \cdots & -S_{2}^{\tilde{n}} \\
-S_{3}^{\tilde{1}} & -S_{3}^{\tilde{2}} & \cdots & -S_{3}^{\tilde{n}}
\end{pmatrix}_{3\times\tilde{n}}, \begin{pmatrix}
S_{1}^{\tilde{n}} & \cdots & S_{1}^{\tilde{2}} & S_{1}^{\tilde{1}} \\
S_{2}^{\tilde{n}} & \cdots & S_{2}^{\tilde{2}} & S_{2}^{\tilde{1}} \\
S_{3}^{\tilde{n}} & \cdots & S_{3}^{\tilde{2}} & S_{3}^{\tilde{1}}
\end{pmatrix}_{3\times\tilde{n}}, \\
\begin{pmatrix}
-S_{1}^{\tilde{n}} & \cdots & -S_{1}^{\tilde{2}} & -S_{1}^{\tilde{1}} \\
-S_{2}^{\tilde{n}} & \cdots & -S_{2}^{\tilde{2}} & -S_{2}^{\tilde{1}} \\
-S_{3}^{\tilde{n}} & \cdots & -S_{3}^{\tilde{2}} & -S_{3}^{\tilde{1}}
\end{pmatrix}_{3\times\tilde{n}}$$
(18)

as the "Negative Merged Shape Matrix", "Inverse Merged Shape Matrix", and "Negative-Inverse Merged Shape Matrix", respectively, corresponding to Merged Shape Matrix (17). All three matrices, in conjunction with the original Merged Shape Matrix (17), delineate the shape of the same trajectory using the identical set of sampling points. The distinction arises from the vantage point from which the mobile trajectory is observed. Furthermore, when focusing exclusively on the horizontal bending and vertical ascending/descending directions of the mobile trajectory, we can define the Sign Matrix for each of these matrices. These Sign Matrices are constructed based on the signs of the elements within the Merged Shape Matrices, offering a concise representation of the trajectory's directional characteristics.

Remark 5 Examining a three-dimensional spatial curve

from alternative angles extends beyond considering only the four cardinal viewing directions: up, down, front, and rear. However, for real-world ground object trajectories, it suffices to project the spatial trajectory of an object onto the horizontal ground surface. Subsequently, observations can be made in both the vertical dimension (up and down) and the longitudinal dimension (front and rear) concerning this mobile trajectory on the horizontal ground surface.

B. Matching Corresponding Points or Parts of a Mobile Trajectory — Utilizing Symbol Overlap Method with Symbol Matrices

When assessing the similarity between two mobile trajectories based on their sampled points, a crucial step is to align and match the corresponding points or parts between them accurately. This process is analogous to the need for identifying corresponding vertices when determining the similarity of two simple triangles. Without appropriately matching the vertices, it becomes challenging to establish the similarity of the triangles. Similarly, when dealing with two mobile trajectories, the correct pairing of points and parts is essential. Given two sets of sampled points from different trajectories, we can employ the "symbol overlap method" to match them effectively.

Assuming two mobile trajectories, denoted as ${\cal C}_{\cal A}$ and ${\cal C}_{\cal B}$, along with their respective sampled points, which correspond to merged shape matrices

$$\begin{pmatrix} S_{1}^{1,\tilde{1}} & S_{1}^{1,\tilde{2}} & \cdots & S_{1}^{1,\tilde{n}} \\ S_{2}^{1,\tilde{1}} & S_{2}^{1,\tilde{2}} & \cdots & S_{2}^{1,\tilde{n}} \\ S_{3}^{1,\tilde{1}} & S_{3}^{1,\tilde{2}} & \cdots & S_{3}^{1,\tilde{n}} \end{pmatrix}_{3\times\tilde{n}} \text{ and } \begin{pmatrix} S_{1}^{2,\tilde{1}} & S_{1}^{2,\tilde{2}} & \cdots & S_{1}^{2,\tilde{m}} \\ S_{2}^{2,\tilde{1}} & S_{2}^{2,\tilde{2}} & \cdots & S_{2}^{2,\tilde{m}} \\ S_{3}^{2,\tilde{1}} & S_{3}^{2,\tilde{2}} & \cdots & S_{3}^{2,\tilde{m}} \end{pmatrix}_{3\times\tilde{n}}$$
(19)

we seek to simplify them into symbol matrices associated with the merged shapes. These symbol matrices are aligned both vertically and horizontally. To establish a match between one of the symbol matrices and the other, we shift them relative to one another. The point in time with the highest number of matching symbols (the symbols are the same) at the overlapping position represents the optimal match between these two matrices. A higher number of matching symbols at the overlapping position indicates a closer resemblance between the shapes of the trajectory segments corresponding to the overlapping position. By determining the optimal match position between the two symbol matrices, we effectively identified the best correspondence between points or parts on the two trajectories. We further extend the matching process by transforming one of the symbol matrices into its negative, inverse, and negative-inverse symbol matrices. These transformed matrices are then overlapped and matched with the other symbol matrix, allowing us to explore alternative optimal trajectory matches.

To facilitate clarity, we illustrate the key concepts and principles of matching using the example of point correspondences in planar trajectories. For instance, consider two planar mobile trajectories C_A and C_B , as illustrated in Fig. 10 . The shorter trajectory has been depicted four times, including its reverse, inverse, and reverse-inverse renditions.

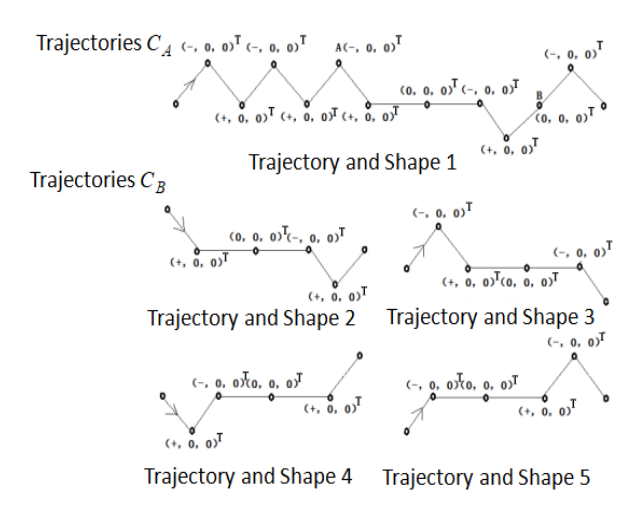


Fig. 10. Two planar trajectories and their local shape symbol vectors.

In Fig. 10, the symbol matrix for the merged shape matrix of "Trajectory and Shape 1" is

while the symbol matrix for the merged shape matrix of "Trajectory and Shape 2" is

$$\begin{pmatrix} + & 0 & - & + \\ 0 & 0 & 0 & 0 \\ 0 & 0 & 0 & 0 \end{pmatrix}$$

The optimal match position for these two matrices was found at points A to B of "Trajectory and Shape 1" in Fig. 10. At this overlapping position, all the symbols in both symbol matrices are identical. In cases where multiple optimal match positions exist (i.e., when the number of matching symbols is the same), all positions are recorded.

Subsequently, the symbol matrix for the merged shape of "Trajectory and Shape 1" is compared with the merged shape symbol matrices of "Trajectory and Shape 3," "Trajectory and Shape 4," and "Trajectory and Shape 5" (i.e., the negative-inverse, inverse, and negative merged shape matrices of "Trajectory and Shape 2"). Record all the optimal match positions.

C. The Similarity of Mobile Trajectories - Measuring Distance Using Post-Matching Filled Matrices

Calculate the distance between the merged shape matrices obtained from all pairwise matches and select the minimum distance as a metric for the similarity between the two trajectories. The procedure is outlined as follows. First, fill the non-overlapping regions of the two merged shape matrices with $(0,0,0)^T$ to extend them to the same order, generating what we will refer to as their "filled matrices". Note that higher-order merged shape matrices may not require filling. Further, calculate the distance between these two filled matrices of the same order.

In specific terms, given two trajectories with merged shape matrices denoted as

$$\begin{pmatrix} S_{1}^{1,\tilde{1}} & S_{1}^{1,\tilde{2}} & \cdots & S_{1}^{1,\tilde{n}} \\ S_{2}^{1,\tilde{1}} & S_{2}^{1,\tilde{2}} & \cdots & S_{2}^{1,\tilde{n}} \\ S_{3}^{1,\tilde{1}} & S_{3}^{1,\tilde{2}} & \cdots & S_{3}^{1,\tilde{n}} \end{pmatrix}_{3\times\tilde{n}} \quad \text{and} \quad \begin{pmatrix} S_{1}^{2,\tilde{1}} & S_{1}^{2,\tilde{2}} & \cdots & S_{1}^{2,\tilde{m}} \\ S_{2}^{2,\tilde{1}} & S_{2}^{2,\tilde{2}} & \cdots & S_{2}^{2,\tilde{m}} \\ S_{3}^{2,\tilde{1}} & S_{3}^{2,\tilde{2}} & \cdots & S_{3}^{2,\tilde{m}} \end{pmatrix}_{3\times\tilde{m}}$$
(20)

and assuming $\widetilde{n} \leq \widetilde{m}$, we posit that the best matching position of the first merged shape matrix within the second one starts from the d-th column of the second merged shape matrix.

If $d-1+\widetilde{n} > \widetilde{m}$, then the first merged shape matrix is expanded into a filled matrix

$$\begin{pmatrix}
0 & \cdots & 0 & S_1^{1,\tilde{1}} & S_1^{1,\tilde{2}} & \cdots & S_1^{1,\tilde{n}} & 0 & \cdots & 0 \\
0 & \cdots & 0 & S_2^{1,\tilde{1}} & S_2^{1,\tilde{2}} & \cdots & S_2^{1,\tilde{n}} & 0 & \cdots & 0 \\
0 & \cdots & 0 & S_3^{1,\tilde{1}} & S_3^{1,\tilde{2}} & \cdots & S_3^{1,\tilde{n}} & 0 & \cdots & 0
\end{pmatrix}.$$
(21)

It has d-1 leading $(0,0,0)^T$ elements and $\widetilde{m}-\widetilde{n}-(d-1)$ trailing $(0,0,0)^T$ elements. The second merged shape matrix does not require filling because it is of the same order as the filled first merged shape matrix.

However, if $d-1+\widetilde{n}>\widetilde{m}$, both merged shape matrices are expanded into filled matrices of equal order, resulting in matrices

$$\begin{pmatrix} 0 & \cdots & 0 & S_1^{1,\widetilde{1}} & S_1^{1,\widetilde{2}} & \cdots & S_1^{1,\widetilde{n}} \\ 0 & \cdots & 0 & S_2^{1,\widetilde{1}} & S_2^{1,\widetilde{2}} & \cdots & S_2^{1,\widetilde{n}} \\ 0 & \cdots & 0 & S_3^{1,\widetilde{1}} & S_3^{1,\widetilde{2}} & \cdots & S_3^{1,\widetilde{n}} \end{pmatrix} \text{and} \quad \begin{pmatrix} S_1^{2,\widetilde{1}} & S_1^{2,\widetilde{2}} & \cdots & S_1^{2,\widetilde{m}} & 0 & \cdots & 0 \\ S_2^{2,\widetilde{1}} & S_2^{2,\widetilde{2}} & \cdots & S_2^{2,\widetilde{m}} & 0 & \cdots & 0 \\ S_3^{2,\widetilde{1}} & S_3^{2,\widetilde{2}} & \cdots & S_3^{2,\widetilde{m}} & 0 & \cdots & 0 \end{pmatrix}$$

as described above. The first matrix contains d-1 leading $(0,0,0)^T$ elements, whereas the second matrix has $d-1+\widetilde{n}-\widetilde{m}$ trailing $(0,0,0)^T$ elements.

After expanding the matched merged shape matrices into filled matrices of the same order, the distance between the two matched merged shape matrices is computed by subtracting the corresponding elements of the filled matrices, squaring them, and summing the results. This yields the distance between the two matched merged shape matrices. To measure the degree of similarity between the two trajectories, we considered the minimum distance among all pairwise-matched merged shape matrices. A smaller distance indicates a higher degree of similarity between the two trajectories, whereas a larger distance suggests a lower degree of similarity. The flowchart in Fig. 11 illustrates the process of calculating the similarity between two mobile trajectories.

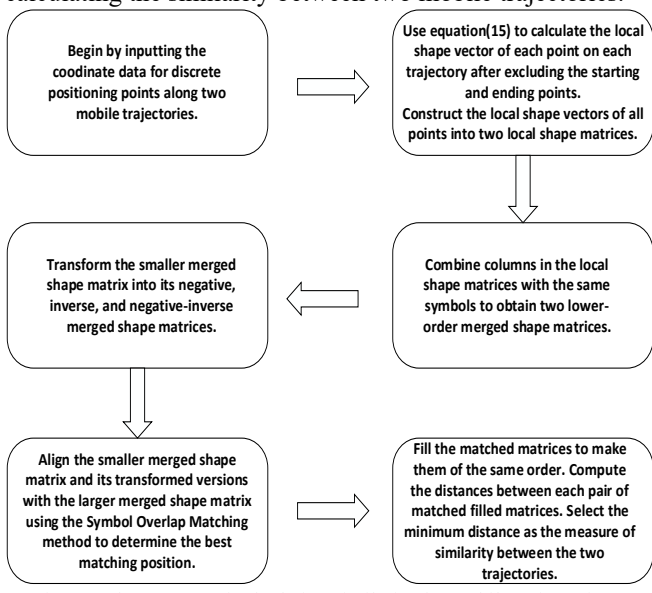


Fig. 11. The process of calculating similarity for mobile trajectories.

Remark 6 The distance between two matched filled matrices of the same order, as described above, is the square of the Euclidean distance between the matrices. It is important to note that in addition to the Euclidean distance, various other distance metrics are available for measuring the difference between matrices. The choice of distance metric should be based on the specific characteristics of the data and the requirements of the research or application. Different distance metrics may be more suitable for different scenarios, and selecting the appropriate metric can have a significant impact on the results and interpretations of your analysis.

IV. CALCULATION EXPERIMENT OF MOVING TRAJECTORY SIMILARITY

To validate the efficacy and practicality of the aforementioned mobile trajectory similarity measurement, we conducted a straightforward yet illustrative experiment using positioning data from moving vehicles. When vehicles are in regular operation, they typically follow smooth trajectories at relatively constant speeds. The positioning data were collected at equidistant time intervals, aligning with the conditions specified in the second formula in expression (15) outlined earlier.

For the purposes of visual comparison, we selected three distinct vehicle trajectories in three-dimension space, denoted as (a), (b), and (c). The positioning data corresponding to these trajectories are succinctly represented in Cartesian coordinates (unit, /m), as presented in Tables I, II, and III. In these tables, 'i' signifies the sequential order of positioning points along the trajectory or the timestamp of data acquisition (unit, /10s). The planar projections of these three trajectories are shown in Fig.12 (a), (b), and (c).

Step 1: Computing Local Shape Vectors for Points 2 through 8 in Table I. As an illustrative example, we demonstrate the computation of the local shape vector for point 2.

(1.1)Calculate the algebraic area of the triangle formed by points 1, 2, and 3 in Table I,

$$\begin{vmatrix} 0 & 0 \\ 30 & 71 \end{vmatrix} + \begin{vmatrix} 30 & 71 \\ 100 & 100 \end{vmatrix} + \begin{vmatrix} 100 & 100 \\ 0 & 0 \end{vmatrix} = -4100$$

TABLE I
The data collection points from trajectory (a)

i	x_i^1	y_i^1	z_i^1
1	0	0	0
2	30	71	2
3	100	100	4
4	170	69	6
5	200	0	8
6	280	0	10
7	358	0	12
8	435	0	14
9	510	0	16

¹ Tables may have footers.

(1.2)Calculate the following for points in Table I. Horizontal distances between points 1 and 2, 2 and 3, and 3 and 1.

$$\sqrt{(30-0)^2 + (71-0)^2} = 77.07788269,$$

$$\sqrt{(100-30)^2 + (100-71)^2} = 75.76938696,$$

$$\sqrt{(0-100)^2 + (0-100)^2} = 141.4213562.$$

Altitude differences between points 1 and 2, 2 and 3. 2-0=2, 4-2=2.

(1.3)Calculate the local shape vector for point 2 using expression (1).

$$\left(\operatorname{sgn}(-4100)\frac{77.07788269 + 75.76938696}{141.4213562}, \frac{2}{77.07788269}, \frac{2}{75.76938696}\right)^{7}$$

In other words, the local shape vector for point 2 is

 $(-1.080793409, 0.025947781, 0.026395885)^{T}$.

TABLE II
The data collection points from trajectory (b)

The data concerton points from trajectory (b)				
i	x_i^2	${\cal Y}_i^2$	z_i^2	
1	101	101	50	
2	212	213	45	
3	154	353	40	
4	212	495	35	
5	354	700	30	
6	495	495	25	

TABLE III
The data collection points from trajectory(c)

i	x_i^3	${\cal Y}_i^3$	z_i^3
1	717	717	15
2	830	830	15
3	940	940	15
4	1050	1050	15

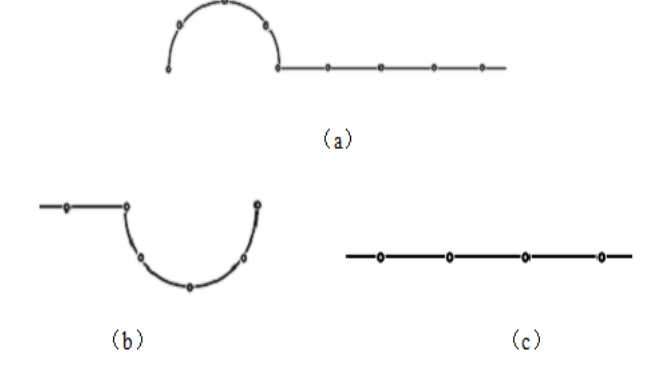


Fig. 12. Plane projection of three different vehicle trajectories.

Following the same procedure as outlined in (1.1) through (1.3), calculate the local shape vectors for the other points in Table I. The resulting local shape vectors for each point are presented in Table IV.

Clearly, the local shape matrix for trajectory (a) is composed of the data in the second column of Table IV. For ease of presentation, we will directly use Table IV to represent the local shape matrix for trajectory (a).

Step 2: Merging the Local Shape Matrices of Trajectory (a) to Obtain the Merged Shape Matrix of Trajectory (a). In this step, we employ Table V to elucidate the merging process of the local shape matrices for trajectory (a).

TABLE IV
Local shape vectors of points in trajectory (a)

the position of points on the trajectory (order number i)	local shape vectors	
2	$(-1.080793409, 0.025947781, 0.026395885)^{T}$	
3	$(-1.087935814, 0.026395885, 0.026124268)^{T}$	
4	$\left(-1.073365363, 0.026124268, 0.026581741\right)^{T}$	
5	$(1.195531158, 0.026581741, 0.025000000)^{T}$	
6	$\big(0.000000000, 0.025000000, 0.025641026\big)^{\! T}$	
7	$ig(0.0000000000, 0.025641026, 0.025974026ig)^{^T}$	
8	$ig(0.0000000000, 0.025974026, 0.0266666667ig)^{\! T}$	

Table V
Concatenation of local shape matrices for trajectory (a)

the position of points on the trajectory (order number <i>i</i>)	the symbol vector corresponding to the local shape vector	the merging of the local shape vectors
2	$(-,+,+)^T$	As these symbols of the three items are the same, merge them into one item
3	$(-,+,+)^T$	$(-3.242094586, 0.078467934, 0.079101894)^T$
4	$(-,+,+)^T$	
5	$(+,+,+)^T$	Merge this item into a new one $(1.195531158, 0.026581741, 0.025000000)^T$
6	$\big(0,+,+\big)^{\! T}$	As these symbols of the three items are the same, merge them into one item
7	$(0,+,+)^T$	$(0.000000000, 0.076615052, 0.078281718)^{T}$
8	$ig(0,+,+ig)^{\!\scriptscriptstyle T}$	

TABLE VI
The merged shape matrix and corresponding symbol matrix for trajectory (a)

the order number after merging shapes	the corresponding symbol matrix	merged shape matrix
1	$(-,+,+)^T$	$\left(-3.242094586, 0.078467934, 0.079101894\right)^{T}$
2	$(+,+,+)^T$	$\left(1.195531158, 0.026581741, 0.025000000\right)^{T}$
3	$(0,+,+)^{T}$	$ig(0.000000000, 0.076615052, 0.078281718ig)^{^T}$

Consequently, we can obtain the merged shape matrix and the corresponding symbol matrix for trajectory (a). Here, we can equivalently use Table VI to represent the merged shape matrix and its corresponding symbol matrix for trajectory (a). They are respectively formed by the data in the third column and the second column of Table VI.

Step 3: Calculating Local Shape Matrices and Merged Shape Matrices (Symbol Matrices are Generated Naturally) for Trajectories (b) and (c). The same process outlined in

Steps 1 and 2 is applied to compute the local shape matrices and merged shape matrices for trajectories (b) and (c). This is represented using Tables VII, VIII, IX, and X.

Step 4: Deriving Negative Matrices, Inverse Matrices, and Negative-Inverse Matrices for the Merged Shape Matrices of Trajectories (b) and (c). For ease of observation and using the Symbol Overlap Matching method, record only their corresponding symbol matrices in Table XI and XII.

IAENG International Journal of Applied Mathematics

TABLE VII

Local shape vectors of points in trajectory (b)

the position of points on the trajectory (order number i)	local shape vectors
2	$(1.200813333, -0.031708505, -0.032994856)^T$
3	$(-1.081302021, -0.032994856, -0.03259699)^{T}$
4	$(-1.005629551, -0.03259699, -0.020049946)^{T}$
5	$(-1.760375930, -0.020049946, -0.020095723)^T$

TABLE VIII

The merged matrix and corresponding symbol matrix for trajectors

the order number after merging shapes	the corresponding symbol matrix	merged shape matrix
1	$(+, -, -)^T$	$(1.200813333, -0.031708505, -0.032994856)^{T}$
2	$(-,-,-)^T$	$(-3.847307501, -0.085641792, -0.072742659)^T$

TABLE IX

the position of points on the trajectory (order number i)	local shape vectors
2	$(0,0,0)^{^T}$
3	$\big(0,0,0\big)^{\! \scriptscriptstyle T}$

TABLE X
The merged matrix and corresponding symbol matrix for trajectory (c)

the order number after merging shapes	the corresponding symbol matrix	merged shape matrix
1	$\big(0,0,0\big)^{\! \scriptscriptstyle T}$	$\big(0,0,0\big)^{\! T}$

TABLE XI

1	Merged shape matrix for trajectory (b) and corresponding symbol matrices for its negative, inverse, and negative-inverse matrices				
the order	merged shape matrix of trajectory (b)	negative merged shape matrix of trajectory (b)	inverse merged shape matrix of trajectory (b)	negative-inverse merged shape matrix of trajectory (b)	
	(symbolic matrix)	(symbolic matrix)	(symbolic matrix)	(symbolic matrix)	
1	$(+, -, -)^T$	$(-,+,+)^T$	$(-,-,-)^T$	$(+,+,+)^T$	
2	$(-,-,-)^T$	$(+,+,+)^T$	$(+, -, -)^T$	$(-,+,+)^T$	

TABLE XII

the order	merged shape matrix of trajectory (c)	negative merged shape matrix of trajectory (c)	inverse merged shape matrix of trajectory (c)	negative-inverse merged shape matrix of trajectory (c)
number	(symbolic matrix)	(symbolic matrix)	(symbolic matrix)	(symbolic matrix)
1	$\big(0,0,0\big)^{\! T}$	$\big(0,0,0\big)^{^{T}}$	$\big(0,0,0\big)^{\! T}$	$(0,0,0)^{^T}$

Table XIII	
Ontimal position matching between trajectory (a) and trajectory (b)	

the order	merged shape matrix	merged shape	negative merged	inverse merged	negative-inverse
number	of trajectory	matrix of trajectory	shape matrix of	shape matrix of	merged shape matrix
			trajectory	trajectory	of trajectory
	(a)	(b)			(b)
	(symbolic matrix)	(symbolic matrix)	(b)	(b)	(symbolic matrix)
			(symbolic matrix)	(symbolic matrix)	
1	$\left(-,+,+\right)^T$	$\big(0,0,0\big)^{\! \scriptscriptstyle T}$	$(-,+,+)^T$	$(-,-,-)^T$	$\big(0,0,0\big)^{\! T}$
		filling			filling
2	$(+,+,+)^T$	$(+,-,-)^T$	$(+,+,+)^T$	$(+, -, -)^T$	$(+,+,+)^T$
3	$ig(0,+,+ig)^T$	$(-,-,-)^T$	$\big(0,0,0\big)^{\! \mathrm{\scriptscriptstyle T}}$	$\big(0,0,0\big)^{\! T}$	$\left(,+,+\right) ^{T}$
5			filling	filling	

TABLE XIV

Optimal position matching between trajectory (a) and trajectory (c)									
the order	merged shape	merged shape	negative merged	inverse merged	negative-inverse				
number	matrix of trajectory	matrix of trajectory	shape matrix of	shape matrix of	merged shape matrix				
			trajectory	trajectory	of trajectory				
	(a)	(c)	(c)	(c)	(c)				
	(symbolic matrix)	(symbolic matrix)	(symbolic matrix)	(symbolic matrix)	(symbolic matrix)				
1	$(-,+,+)^T$	$\big(0,0,0\big)^{\! \scriptscriptstyle T}$	$ig(0,0,0ig)^{\! T}$	$\big(0,0,0\big)^{\! T}$	$\big(0,0,0\big)^{\! \scriptscriptstyle T}$				
		filling	filling	filling	filling				
2	$(+,+,+)^T$	$\big(0,0,0\big)^{\! T}$	$(0,0,0)^{T}$	$\big(0,0,0\big)^{\! T}$	$\big(0,0,0\big)^{\! T}$				
		filling	filling	filling	filling				
3	$(0,+,+)^T$	$\big(0,0,0\big)^{\! \scriptscriptstyle T}$	$\big(0,0,0\big)^{\! \scriptscriptstyle T}$	$\big(0,0,0\big)^{\! T}$	$\big(0,0,0\big)^{\! \scriptscriptstyle T}$				

Step 5: Matching Trajectories (b) and (c) with Trajectory (a) and Calculating the Similarity of Trajectories. Taking the matching of trajectory (b) with trajectory (a) as an example, this process involves matching the merged shape symbol matrix of trajectory (a) with the merged shape symbol matrix of trajectory (b) and its negative, inverse, and negative-inverse merged shape symbol matrices. The matrices are subsequently filled to become matrices of the same order. This is depicted in Table XIII.

The degree of similarity between trajectory (a) and trajectory (b) is quantified by the minimum distance between two matched filled matrices of the same order. We illustrate this by calculating the distance between the two matrices found in columns 2 and 3 of Table XIII above.

Similarly, we can compute the following distances:

Distance between columns 2 and 4 of Table XIII: 3.457493481344650.

Distance between columns 2 and 5 of Table XIII: 0.759965907770135.

Distance between columns 2 and 6 of Table XIII: 6.156688677791080.

We select the minimum distance among all matched matrix pairs as the measure of similarity between trajectory (a) and trajectory (b). Therefore, the similarity between trajectory (a) and trajectory (b) is represented as 0.759965907770135.

By performing a similar matching procedure for trajectory (a) and trajectory (c), and calculating their similarity, we obtain the following:

Taking the minimum distance among all matched matrix pairs as the measure of similarity between trajectory (a) and trajectory (c), we denote the similarity between trajectory (a) and trajectory (c) as

=3.45922185785241.

Since 3.45922185785241 is greater than 0.759965907770135, we can conclude that trajectory (b) is more similar to trajectory (a) than trajectory (c) is to trajectory (a). Observing Fig. 12 (a), (b), and (c), it is evident that trajectory (b) and (a) are more similar than trajectory (c) and (a), aligning with the intuitive observations, thus validating our computational results.

V. CONCLUSIONS

In this paper, we investigate the characteristics of real-world object movement trajectories on the Earth's surface. Drawing on geometric theory, we construct measures to capture the local shape of mobile trajectories—specifically, the local shape vector and local shape matrix. We further introduce a measure to characterize the overall shape of mobile trajectories, referred to as the merged shape matrix. Correspondingly, symbolic vectors and matrices are proposed to represent the coarse shape of these trajectories.

Additionally, we propose a Symbol Overlap Method for matching corresponding points or segments between two mobile trajectories. The similarity between mobile trajectories is quantified using the distance between their matched merged shape matrices. This metric emphasizes the geometric properties of the trajectories while effectively addressing the challenge of aligning corresponding points or segments. Notably, the method does not require large-scale data or pre-training of deep representation models. Even with limited trajectory data, it reliably computes similarity between trajectories. As location-based services continue to grow in prevalence, this methodology is positioned to serve as a valuable tool for measuring the similarity of mobile trajectories.

REFERENCES

- Gao, Q.; Zhang, F.L.; Wang, R.J.; Zhou, F. Trajectory big data: A review of key technologies in data processing. J. Softw. 2017, 28, 959-992.
- [2] Zheng, Y. Trajectory Data Mining. ACM Trans. Intell. Syst. Technol. 2015, 6, 1-41.
- [3] Fan, Q.; Zhang, D.X.; Wu, H.Y.; Tan, K.L. A general and parallel platform for mining co-movement patterns over large-scale trajectories. Proc. VLDB Endow. 2016, 10, 313-324.
- [4] Xu, J.J.; Zheng, K.; Chi, M.M. Trajectory big data: data, applications and techniques. J. Commun. 2015, 36, 97-105.
- [5] Huang, X.J.; Liu, Z.X. Method and device for identifying frequent lane changes of vehicles based on sparse satellite positioning data. Chinese Patent ZL202110839025.0, 12 July 2022.
- [6] Liu, J.Y.; Guo, Q.; Chen, J.Y. A Method for Measuring the Similarity of Sea Target Trajectory Based on the Improved Frechet Distance. Radio Eng. 2022, 52, 1080-1085.
- [7] Li, X.; Zhao, K.; Cong, G. Deep representation learning for trajectory similarity computation. In Proceedings of the IEEE 34th International Conference on Data Engineering (ICDE), Paris, France, 16–18 April 2018; pp. 617-628.
- [8] Zhang, Y.; Liu, A.; Liu, G. Deep representation learning of activity Trajectory similarity computation. In Proceedings of the IEEE International Conference on Web Services (ICWS), Milan, Italy, 8– 13 July 2019; pp. 312-319.
- [9] Toohey, K.; Duckham, M. Trajectory similarity measures. SIGSPATIAL Spec. 2015, 7, 43-50.
- [10] Huttenlocher, D.P.; Klandermang, G.A.; Rucklidgew, W.J. Comparing images using the Hausdorff distance. IEEE Trans. Pattern Anal. Mach. Intell. 1993, 15, 850-863.
- [11] Alt, H.; Godau, M. Computing the Fréchet Distance between Two Polygonal Curves. Int. J. Comput. Geom. Appl. 1995, 5, 75-91.
- [12] Zhang, Z.G.; Zhao, X.M. Preliminary study on similarity of plane curves. J. Tianjin Norm. Univ. (Nat. Sci. Ed.) 1998, 18, 65-72.
- [13] Wu, D.R. Lectures on Differential Geometry, 4th ed.; Higher Education Press: Beijing, China, 1981.
- [14] Zhang, Z.S. New Lectures on Mathematical Analysis; Peking University Press: Beijing, China, 1990.
- [15] Falconer, K. Fractal Geometry: Mathematical Foundations and Applications; Wiley: New Jersey, USA, 1990.
- [16] Xia, D.X.; Wu, Z.R.; Yan, S.Z.; Shu, W.C. Real Variable Function Theory and Functional Analysis, 2nd ed.; Higher Education Press: Beijing, China, 2010.
- [17] Dubuissonm, P.; Jain, A.K. A modified Hausdorff distance for object matching. In Proceedings of the IEEE International Conference on Pattern Recognition, Jerusalem, Israel, 9–13 October 1994; pp. 566-568.

- [18] Lu, Y.; Tan, C. Chinese word searching in imaged documents. Int. J. Pattern Recognit. Artif. Intell. 2004, 18, 229-246.
- [19] Buchin, K.; Buchin, M.; Wenk, C. Computing the Fréchet distance between simple polygons. Comput. Geom. 2008, 41, 2-20.
- [20] Avraham, R.B.; Filtser, O.; Kaplan, H. The Discrete and Semicontinuous Fréchet Distance with Shortcuts via Approximate Distance Counting and Selection. ACM Trans. Algorithms 2015, 11, 1-29.
- [21] Wang, L. Counterexamples in Real Analysis; Higher Education Press: Beijing, China, 2014.
- [22] Calin, O. Deep Learning Architectures-A Mathematical Approach; Springer: Cham, Switzerland, 2020.
- [23] Goodfellow, I.; Bengio, Y.; Courville, A. Deep Learning; MIT Press: Cambridge, MA, USA, 2016.
- [24] LeCun, Y.; Bottou, L.; Bengio, Y.; Haffner, P. Gradient based learning applied to document recognition. Proc. IEEE 1998, 86, 2278-2324.
- [25] Tariq, R. Make Your Own Neural Network; CreateSpace Independent Publishing Platform: Charleston, SC, USA, 2016.
- [26] Yao, M.; Zhang, C.; Zhu, Z.H. Trajectory Clustering via Deep Representation Learning. In Proceedings of the International Joint Conference on Neural Networks, Anchorage, AK, USA, 14–19 May 2017; pp. 3880-3887.
- [27] Ruijin Li, and Jianzhong Cui, "On the Wiener Index of Graphs with Predetermined Dissociation Number," IAENG International Journal of Applied Mathematics, vol. 55, no. 6, pp1604-1608, 2025.
- [28] Zhuan Liu, and Peng Gao, "Statistical Inference for Uncertain Intelligent Transportation Systems from Discrete Observations," IAENG International Journal of Applied Mathematics, vol. 55, no. 5, pp1138-1145, 2025.
- [29] Saraswathi D, Britto Antony Xavier G, Abisha M, and Abirami V, "Delta Alpha Integration In Discrete Fractional Calculus," IAENG International Journal of Applied Mathematics, vol. 55, no. 4, pp855-860, 2025.